International Journal of Heat and Fluid Flow 82 (2020) 108554

Contents lists available at ScienceDirect

International Journal of Heat and Fluid Flow

journal homepage: www.elsevier.com/locate/ijhff

Reduced order model of offshore wind turbine wake by proper orthogonal decomposition

M. Salman Siddiqui[*,a], Sidra Tul Muntaha Latif[b], Muhammad Saeed[c], Muhammad Rahman[d], Abdul Waheed Badar[e], Syed Maaz Hasan[f]

[a] Department of Architecture & Technology, Norwegian University of Science & Technology, Trondheim, Norway
[b] Department of Computer Science, Norwegian University of Science & Technology, Trondheim, Norway
[c] Department of Mechanical Engineering, Kyungpook National University, Daegu, Korea
[d] Department of Mathematics Mirpur University of Science and Technology, Mirpur Aj&k, Pakistan
[e] Department of Mechanical Engineering, HITEC University, Taxila, Pakistan
[f] Department of Mechanical Engineering, College of Electrical & Mechanical Engineering, Rawalpindi, Pakistan

ARTICLE INFO

Keywords:
Wind Energy
Proper Orthogonal Decomposition
Reduced Order Models
High Fidelity Simulations
High Reynolds Number Flows
Sliding Mesh Interface
NREL 5MW Offshore Wind Turbine
Wake Dynamics

ABSTRACT

A wide range of previously designed methods for faster parametrization of partial differential equations requires them to be solved using existing finite volume, finite element, and finite difference solvers. Due to the requirement of high degrees of freedom to accurately model the physical system, computational costs often becomes a bottle-neck. It poses challenges to conducting efficient repeated parametric sampling of the input parameter that disrupts the whole design process. Model reduction techniques adopted to high fidelity systems provide a basis to accurately represent a physical system with a lower degree of freedom. The present work focuses on one such method for high-fidelity simulations that combines finite volume strategy with proper orthogonal decomposition and Galerkin projection to test reduced-order models for high Reynolds number flow applications. The model is first benchmarked against flow around a cylinder for which extensive numerical and experimental data is available in the literature. The models are then tested to full-scale NREL 5MW offshore wind turbines to evaluate wake evolution in the downstream direction. The simulations results show relative errors of wind turbines for the first seventy modes approach 4.7% in L^2-norm for velocities.

1. Introduction

Wind power has witnessed tremendous growth over the last two decades. According to H.Kazimierczuk (2019), the global installed capacity has reached to almost 600 GW at the end of 2018 Siddiqui et al. (2019b). In this regard, wind turbines potential has been exalted by restricting their operation to close proximity, thereby enabling maximal gains from sites having enormous wind potential (Sørensen and Zahle, 2016; Tabib et al., 2017b). Although dense layouts have affected the wind power business positively, nevertheless, from an engineering standpoint, such tight placement has given rise to complex flow characterization, analysis of which is paramount for successful long-term operations of a wind park (Siddiqui et al., 2017c). To study this complex dynamic flow interaction requires highly sophisticated tools in the form of experimental, analytical, or numerical techniques. Large sizes of modern wind turbines restrict such experimental investigation owing to limited cross-sections of wind tunnels (Siddiqui et al., 2017b). On the other hand, analytical methods developed through various approximations are not considered suitable to obtain realistic estimates of aerodynamic loads (Siddiqui et al., 2020). Numerical modelings approach at this point provides an efficient alternative - thanks to the immense computational power of modern supercomputers (Siddiqui et al., January 5-11, 2017; Troldborg et al., 2015; Krogstad and Saetran, 2012). Such methods are capable of analyzing turbines in fully resolved high fidelity numerical settings. However, given the need to employ these methods for optimization/control problems which require repeated sampling of field variable to draw parametric estimates, the numerical procedures still become exhaustive even for the most advanced scientific computing clusters (Tabib et al., 2017a; Rozza, 2015; Siddiqui et al., 2019a).

Recently, Reduced Order Modeling (ROM) is getting significant attention for engineering applications (Khalid et al., 2014; Fonn et al., 2017). They offer a unique ability to parametrizes time-dependent Partial Differential Equations (PDEs) for flow-related problems that

* Corresponding author.
E-mail address: muhammad.siddiqui@ntnu.no (M.S. Siddiqui).

https://doi.org/10.1016/j.ijheatfluidflow.2020.108554
Received 9 July 2019; Received in revised form 13 January 2020; Accepted 18 January 2020

have been previously solved using Finite Volume (FV) Zahoor et al. (2028, 2018), Finite Element (FE), and Finite Difference (FD) solvers (Mandar Tabib, 2017; Patera and Rønquist, 2007). The construction of such methods is associated with a single time computational cost of high fidelity solutions in the offline phase. The solutions can be stored at each parametric value in the form of a flow snapshot matrix. Once a reasonable database is constructed, Greedy Methods (Centroidal Voronoi Tessellations (CVT) Taylor, Lagrange, Hermite, and Proper Orthogonal Decomposition (POD) Proper Generalized Decomposition (PGD)) are applied to obtain basis/modes that constitute of a major part of system energy (Khalid et al., 2015). The new basis is then projected on the governing equations through a Galerkin approach to obtain ROM. The resulting system is capable of approximating its high fidelity counterpart, in the online stage, with reasonable accuracy and in a relatively short time.

The application of the first use of POD to an engineering problem is found in the study (Bakewell and Lumley, 1967; Berkooz et al., 1993) to identify the flow structures of variable spatial length and sizes. Subsequently, (Sirovich, 1987; Aubry, 1991) employed them to analyze the flow in the boundary layer along with turbulence characteristics. The author (Akhtar et al., 2007; 2009) used these techniques to develop snapshots using direct numerical solver and analyzed the characterization of the turbulent structure around cylindrical structures and tandem foils. The authors in (Bastine et al., 2014) employ POD to study wakes of wind turbines. The authors in (Tallet et al., 2015) used this technique to develop velocity-pressure coupled ROM parametrizing the Navier Stokes (NS) equations. The authors (Ballarin et al., 2015a) have provided a substantial contribution to POD by an enrichment procedure that adds supremizer to velocity space and satisfied the inf-sup Ladyzhenskaya Babuska Brezzi (LBB) condition. The author of (Lorenzi et al., 2016b; Stabile et al., 2017a; Lorenzi et al., 2016a; Stabile et al., 2018) further improved the methods to develop ROM through direct integration with finite volume methods capable of analyzing moderate to high Reynolds (Re) number engineering flows.

In this article, the aim is to explore the wake dynamics behind NREL 5MW offshore reference wind turbines through a comparison of high fidelity and low fidelity (ROM solution) solutions by adopting methodology presented in (Stabile et al., 2017b). Full-order finite volume approximations are employed using OpenFOAM® (OF®) to conduct high fidelity simulation performed with a Sliding Mesh Interface (SMI) technique. The coherent wake structures are analyzed by applying the POD technique, which extracts the reduce basis with dominant modes corresponding to higher eigenvalues. The high fidelity solution is projected onto a reduced basis, and the field variable (velocity and pressure) is reconstructed and compared against the full model solution. The results are initially validated against the available numerical and analytical results in the literature (Hsu et al., 2014; Jonkman et al., 2005, Tech. Rep. NREL/EL-500-38230). The POD procedure is applied, and the modes are qualitatively discussed by the coherence in the flow field. The ROM implementation is then discussed, followed by the comparison of results through outlining the spectrum, L^2 error and speedups. The wake is reconstructed on a plane passing through the turbine center, and a detailed comparison (quantitative and qualitative) is presented for a full-scale problem. The present results of exploring the possibilities for a full-scale wind turbine is novel, and to the best of the author's knowledge is described the first time. The complete problem is presented in a well defined and three-dimensional manner of reduced basis method, unlike previous investigations that usually adopt two-dimensional procedures to reduce computational complexity (Troldborg et al., 2015; Krogstad and Saetran, 2012; Siddiqui et al., 2016). This research is expected to motivate the wind engineers working in the field to adopt online/offline ROM strategy to compute faster wake's loading downstream of wind turbines.

The present manuscript is organized as follows. In section 2, a comprehensive overview of the theoretical framework employed in the present work is summarized. Section 3 describes the complete high fidelity numerical solution of the wind turbine and formulation of ROM online/offline strategy along with discussion. Section 4 highlights the main findings of the present work along with future outlooks.

2. Theory

2.1. Governing equations

Flow field around stationary and dynamic objects is governed by PDEs. For the present case, the equations are classified as parametrized incompressible unsteady NS equations. These constitute of standard laws of conservation of momentum and continuity equations and are described as follows.

$$-\nu\Delta\boldsymbol{u} + (\boldsymbol{u}\cdot\nabla)\boldsymbol{u} + \nabla p = \boldsymbol{f} \qquad \text{in } \Omega \tag{1}$$

$$\nabla\cdot\boldsymbol{u} = 0 \qquad \text{in } \Omega \tag{2}$$

$$\boldsymbol{u} = \boldsymbol{g} \qquad \text{on } \Gamma_D \tag{3}$$

$$-p\boldsymbol{n} + \nu(\nabla\boldsymbol{u})\boldsymbol{n} = \boldsymbol{h} \qquad \text{on } \Gamma_N. \tag{4}$$

In an Eulerian context ν is the fluid kinematic viscosity, $\boldsymbol{u}$ is the flow velocity vector, p is the normalized pressure.

2.2. Finite volume (FV) discretization

The equations described in the previous sections are written in conservative form. To discretize respective terms, FV framework is adopted that convert volume integrals to surface integrals. An advantage of FV method is that it ensures local enforcement of the conservative law. The discretization of each term of the governing equations is presented as follows

$$\int_V (\boldsymbol{u}\cdot\nabla)\boldsymbol{u}\, dV - \nu\int_V \Delta\boldsymbol{u}\, dV + \int_V \nabla p\, dV = 0 \tag{5}$$

Applying Gauss theorem to discretize the volume integrals into surface integrals

$$\int_V (\boldsymbol{u}\cdot\nabla)\boldsymbol{u}\, dV = \int_V \nabla\cdot(\boldsymbol{u}\boldsymbol{u})\, dV = \int_S d\boldsymbol{S_f}\cdot(\boldsymbol{u}\boldsymbol{u}) \approx \sum_f \boldsymbol{S_f}\cdot\boldsymbol{u_f}\boldsymbol{u_f} = \sum_f F\boldsymbol{u_f} \tag{6}$$

The Laplacian, continuity and pressure terms are also similarly discretized

$$\int_V \nabla\cdot(\nu\nabla\boldsymbol{u})\, dV = \int_S d\boldsymbol{S_f}\cdot(\nu\nabla\boldsymbol{u}) \approx \sum_f \nu\boldsymbol{S_f}\cdot(\nabla\boldsymbol{u})_f = \nu\sum_f F \tag{7}$$

$$\int_V \nabla\cdot\boldsymbol{u}\, dV = \int_S d\boldsymbol{S}\cdot(\boldsymbol{u}) = \sum_f \boldsymbol{S_f}\cdot\boldsymbol{u_f} = \sum_f F \tag{8}$$

$$\int_V \nabla p\, dV = \int_S d\boldsymbol{S}\cdot(p) = \sum_f \boldsymbol{S_f}\cdot p \tag{9}$$

p represents the values at the center of each control face of the control volume. $\boldsymbol{u_f}$ is the velocity vector evaluated at the center of each face of the control volume. F is the max flux through each face (for further details readers may review (Stabile et al., 2017b))

2.2.1. Rotor and turbulence modeling

The turbine rotation is handled through accurate yet computationally expensive Sliding Mesh Interface (SMI) technique. This procedure model flow around turbine by moving the mesh at the rate of prescribed rotational speed and computing solution at each new time instant (Mo et al., 2013; Siddiqui et al., 2017a).The governing equations of continuity and momentum are described as follows:

$$\frac{\partial\boldsymbol{u}}{\partial t} + \nabla\cdot((\boldsymbol{u}-\boldsymbol{u_g})\otimes\boldsymbol{u}) + \nabla\cdot(\nu+\nu_t)(\nabla\boldsymbol{u} + (\nabla\boldsymbol{u})^{\mathrm{T}}) - \nabla p = \mathbf{f} \tag{10}$$

$$\nabla\cdot(\boldsymbol{u}-\boldsymbol{u_g}) = 0 \tag{11}$$

Here $\boldsymbol{u}$ is the fluid velocity and $\boldsymbol{u_g}$ is the grid velocity (which is zero for the static part of grid), p the fluid pressure, ν and ν_t are the fluid viscosity and the turbulent eddy-viscosity, respectively and $\mathbf{f}$ applied volume forces.

2.3. Turbulence modeling

For what concerns the industrial nature of modeling of turbulent flow (wind turbine in the present case) Unsteady Reynolds Average Navier Stokes (URANS) solution of governing equations is deemed sufficient in comparison to Direct Numerical Simulation (DNS) or Large Eddy Simulation (LES) owing to exhaustive computational requirements of latter for complex geometries for achieving the desired accuracy (Siddiqui et al., 2015a). To model the turbulent stress for the closure of turbulence quantities ($\nu + \nu_t$) arising from Reynolds averaging k-ω Shear Stress Transport (SST) is employed given by the following set of k and ω equations (Menter, 2009)

$$\frac{\partial k}{\partial t} + \nabla\cdot((\mathbf{u} - \mathbf{u_g}) \otimes\ k) = \tau_{ij}\nabla\mathbf{u} + \nabla\cdot\left[\frac{\nu + \nu_t}{\sigma_k}\right](\nabla k + (\nabla k)^{\mathrm{T}}) - \omega k \tag{12}$$

$$\frac{\partial \omega}{\partial t} + \nabla\cdot((\mathbf{u} - \mathbf{u_g}) \otimes\ \omega) = \frac{\gamma}{\nu_t}\tau_{ij}\nabla\mathbf{u} + \nabla\cdot\left[\frac{\nu + \nu_t}{\sigma_\omega}\right](\nabla\omega + (\nabla\omega)^{\mathrm{T}}) - \omega^2\beta + 2(1 - F_1)\frac{\sigma_{\omega 2}}{\omega}\nabla k\nabla\omega \tag{13}$$

Standard model damping functions, auxilliary relations and the trip terms are employed as defined in Menter (1994)

2.4. Reduced Order Model (ROM) construction

The present reduced order modeling strategy is motivated from the study (Lorenzi et al., 2016a) in which the methods for developing ROM based on finite volume applications are proposed. Similar reduced basis space is constructed to approximate solution $\boldsymbol{u_r}(\boldsymbol{x}, t)$ as a linear combination of basis function consisting of the spatial distribution of modes $\boldsymbol{\phi_i(x)}$ with the product to $a_i(t)$ (Ballarin et al., 2015b). For the field variable of velocity, flux, and viscosity becomes

$$\boldsymbol{u}(\boldsymbol{x}, t) \approx \boldsymbol{u}_r(\boldsymbol{x}, t) = \sum_{i=1}^{N_r} a_i(t)\boldsymbol{\phi}_i(\boldsymbol{x}) \tag{14}$$

$$F(\boldsymbol{x}, t) \approx F_r(\boldsymbol{x}, t) = \sum_{i=1}^{N_r} a_i(t)\Psi_i(\boldsymbol{x}) \tag{15}$$

$$p(\boldsymbol{x}, t) \approx p_r(\boldsymbol{x}, t) = \sum_{i=1}^{N_r} a_i(t)\chi_i(\boldsymbol{x}) \tag{16}$$

The spatial basis developed for the velocity, flux and pressure are $\boldsymbol{\phi}_i(\boldsymbol{x})$, $\boldsymbol{\Psi}_i(\boldsymbol{x})$, $\boldsymbol{\chi}_i(\boldsymbol{x})$ respectively, and are constructed from the combination of snapshots computed by high fidelity simulation through Unsteady Reynolds Averaged Navier Stokes (URANS) calculations over various time instants ($i = 1, ...,N_r$) to construct the snapshot matrix of velocity as $\boldsymbol{u_n}(\boldsymbol{x}) = \boldsymbol{u}(\boldsymbol{x}, t_n)$, $n = 1, ...,N_s$. The POD is applied such that the difference between full order snapshot and projection of snapshots with spatial modes in the X-norm (Bizon and Continillo, 2012) remain minimum in L^2

$$X_{Nr}^{POD} = arg\ min\frac{1}{N_s}\sum_{n=1}^{N_s}||\boldsymbol{u}_n(\boldsymbol{x}) - \sum_{i=1}^{N_r}\langle\boldsymbol{u}_n(\boldsymbol{x}), \boldsymbol{\phi}_i(\boldsymbol{x})\rangle||_{L^2}^2 \tag{17}$$

A Singular Value Decomposition (SVD) strategy could be employed to construct the basis, however it has been found to increase the dimensions of grid employed for the discretization of domain (Stabile et al., 2018). Therefore, a similar and more efficient technique in the form of eigen value decomposition is employed. The correlation matrix is thus constructed using the ensemble solutions

$$\langle\boldsymbol{\phi}_i(\boldsymbol{x}), \boldsymbol{\phi}_j(\boldsymbol{x})\rangle_{H_1} = C_{ij} \tag{18}$$

Using the eigenvalue problem approach the matrix is written as

$$C\zeta_i = \lambda_i\zeta_i \quad i = 1, ...,N_s \tag{19}$$

The closeness of the performed approximation is calculated in a specific norm $\|\cdot\|_a$, where squaring this norm determine the variance in the solution. The inner product $\langle\cdot,\ \cdot\rangle_a$ induces the norm and corresponds to covariance. The covariance matrix is determined as

$$[C]_{kl} = \frac{1}{N_r}\langle\boldsymbol{u}_k(\boldsymbol{x}, \boldsymbol{u}_l(\boldsymbol{x})\rangle_{L^2} \tag{20}$$

The eigenpairs of the following matrix ($\boldsymbol{q_i}, \lambda_i$) provide the modes ζ_i such that

$$\zeta_i = \frac{1}{\sqrt{\lambda_i}}\sum_j q_i^j\boldsymbol{\varphi}_j.$$

The (λ_i, ζ_i) eigen value and vector pair enable to construct the POD basis for velocity field in the following manner

$$\boldsymbol{\phi}_i(\boldsymbol{x}) = \frac{1}{\sqrt{\lambda_i}}\sum_{n=1}^{N_s}\zeta_{i,n}\boldsymbol{u}_n(\boldsymbol{x}) \quad i = 1, ...N_r \tag{21}$$

Similarly, for face flux $\boldsymbol{\chi_i(x)}$ and pressure $\boldsymbol{\Psi_i(x)}$, spatial basis is constructed using the eigenvalue decomposition from the full order model.

$$\Psi_i(\boldsymbol{x}) = \frac{1}{\sqrt{\lambda_i}}\sum_{n=1}^{N_s}\zeta_{i,n}F_n(x) \quad i = 1, ...,N \tag{22}$$

$$F_n(x) := F(\boldsymbol{x}, t_n) \quad n = 1, ...,N_s \tag{23}$$

$$\chi_i(\boldsymbol{x}) = \frac{1}{\sqrt{\lambda_i}}\sum_{n=1}^{N_s}\zeta_{i,n}p_n(\boldsymbol{x}) \quad i = 1, ...,N_s \tag{24}$$

$$p_n(\boldsymbol{x}) := p(\boldsymbol{x}, t_n) \quad n = 1, ...,N_s \tag{25}$$

For interpretation, the present approach considers the system as if the state vector is developed as the linear combination of state vector spatial modes (Bergmann et al., 2009).

$$\begin{pmatrix}\mathbf{u}(\mathbf{x}, \mathbf{t})\\ \mathbf{F}(\mathbf{x}, \mathbf{t})\\ p\ (\mathbf{x}, \mathbf{t})\end{pmatrix} \approx \begin{pmatrix}\mathbf{u_r}(\mathbf{x}, \mathbf{t})\\ \mathbf{F_r}(\mathbf{x}, \mathbf{t})\\ p_r\ (\mathbf{x}, \mathbf{t})\end{pmatrix} = \sum_{i=1}^{N_r} a_i(t)\begin{pmatrix}\mathbf{\Phi_i}(\boldsymbol{x})\\ \Psi_i(\boldsymbol{x})\\ \chi_i\ (\boldsymbol{x})\end{pmatrix} \tag{26}$$

To construct the ROM, Galerkin projection is applied to the system of equation through POD basis. Note that since the purpose here is not to evaluate the parameterized variation of the boundary conditions, therefore parameterized condition at the boundaries for velocity are not taken into consideration

$$\frac{da_j(t)}{dt} = \nu\sum_{i=1}^{N_r}B_{ji}a_i(t) - \sum_{k=1}^{N_r}\sum_{i=1}^{N_r}C_{jki}a_k(t)a_i(t) - \sum_{i=1}^{N_r}A_{ji}a_i(t) \quad j = 1, ...,N_r \tag{27}$$

where

$$B_{ji} = \langle\boldsymbol{\phi}_j, \Delta\boldsymbol{\phi}_i\rangle_{L^2} \tag{28}$$

$$C_{jki} = \langle\boldsymbol{\phi}_j, \nabla\cdot(\Psi_k, \boldsymbol{\phi}_i)\boldsymbol{\phi}_i\rangle_{L^2} \tag{29}$$

$$A_{ji} = \langle\boldsymbol{\phi}_j, \nabla\chi_i\rangle_{L^2} \tag{30}$$

The system with corresponding ROM matrices thus becomes

$$\dot{\boldsymbol{a}} = \nu\boldsymbol{Ba} - \boldsymbol{a}^T\boldsymbol{Ca} - \boldsymbol{Aa} \tag{31}$$

Turbulence is added to develop ROM procedure for the present system of highly turbulent flow around wind turbine to conduct efficient simulations at high Re number. For the present case of URANS in FV framework, turbulent viscosity is already embedded in the governing system of equations, thus only eddy viscosity is expanded as a linear combinations of spatial modes as described in Lorenzi et al. (2016a).

$$\nu(\boldsymbol{x}, t) \approx \nu_{t,r}(\boldsymbol{x}, t) = \sum_{i=1}^{N_r} a_i(t)\varphi_i(\boldsymbol{x}) \tag{32}$$

where $\phi_i(x)$ are spatial basis for the eddy viscosity, which are expanded similar to procedure conducted for velocity, pressure and face flux previously. Thus the eigen values and vector reads

$$\phi_i(x) = \frac{1}{\sqrt{\lambda_i}} \sum_{n=1}^{N_s} \xi_{i,n}\nu_n(\boldsymbol{x}) \quad i = 1, ...,N_s \tag{33}$$

$$\nu_n(\boldsymbol{x}) := \nu(\boldsymbol{x}, t_n) \quad n = 1, ...,N_s \tag{34}$$

The time dependent coefficients for turbulent problem becomes

$$\begin{pmatrix} \mathbf{u}(\mathbf{x}, \mathbf{t}) \\ \mathbf{F}(\mathbf{x}, \mathbf{t}) \\ p\ (\mathbf{x}, \mathbf{t}) \\ \nu_t\ (\mathbf{x}, \mathbf{t}) \end{pmatrix} \approx \begin{pmatrix} \mathbf{u_r}(\mathbf{x}, \mathbf{t}) \\ \mathbf{F_r}(\mathbf{x}, \mathbf{t}) \\ p_r\ (\mathbf{x}, \mathbf{t}) \\ \nu_{t,r}\ (\mathbf{x}, \mathbf{t}) \end{pmatrix} = \sum_{i=1}^{N_r} a_i(t) \begin{pmatrix} \mathbf{\Phi_i}(\mathbf{x}) \\ \Psi_i(\mathbf{x}) \\ \chi_i\ (\mathbf{x}) \\ \phi_i\ (\mathbf{x}) \end{pmatrix} \tag{35}$$

Hence for the ROM equations after application of POD from the URANS solution with turbulent term becomes

$$\frac{da_j(t)}{dt} = \nu \sum_{i=1}^{N_r} B_{ji}a_i(t) + \nu \sum_{i=1}^{N_r} BT_{ji}a_i(t) - \sum_{k=1}^{N_r}\sum_{i=1}^{N_r} C_{jki}a_k(t)a_i(t) + \sum_{k=1}^{N_r}\sum_{i=1}^{N_r} CT1_{jki}a_k(t)a_i(t) + \sum_{k=1}^{N_r}\sum_{i=1}^{N_r} CT2_{jki}a_k(t)a_i(t) \tag{36}$$

the additional terms arising from the incorporation of eddy viscosity are represented as

$$BT_{ji} = \langle \boldsymbol{\phi}_j, \nabla\cdot(\nabla\boldsymbol{\phi}_i^T)\rangle_{L^2} \tag{37}$$

$$CT1_{jki} = \langle \boldsymbol{\phi}_j, \phi_k\Delta\boldsymbol{\phi}_i^T\rangle_{L^2} \tag{38}$$

$$CT2_{jki} = \langle \phi_j, \nabla\cdot\phi_k(\nabla\boldsymbol{\phi}_i^T)\rangle_{L^2} \tag{39}$$

The dynamical system that includes the eddy viscosity is modeled as

$$\dot{\boldsymbol{a}} = \nu(\boldsymbol{B} + \boldsymbol{BT})\boldsymbol{a} - \boldsymbol{a}^T(\boldsymbol{C} - \boldsymbol{CT1} - \boldsymbol{CT2})\boldsymbol{a} - \boldsymbol{Aa} + \tau(\boldsymbol{u_{BC}D} - \boldsymbol{Ea}) \tag{40}$$

The advantage of adopted procedure, in the context of present work, is that it does not impart a stringent requirement on turbulent modeling. Moreover, it is applicable to the high fidelity simulations carried out with wall functions. The non-linear term arising in Eq. 40 are crucial and discretized with the backward Euler method (Milosevic, 2018) while the resulting non-linear system is solved using a Newton Iteration procedure (Kumar et al., 2013). Once the solution is, the velocity field is approximated over a plane using Eq. 35 to capture wake.

3. Computational setup

3.1. CAD model

The CAD model of the NREL 5MW turbine is developed using an open-source description of the geometric data given in Jonkman et al. (2005, Tech. Rep. NREL/EL-500-38230). The turbine has three blades comprising of Delft University (DU) and National Advisory Committee for Astronautics (NACA) airfoil sections, i.e., DU21, DU25, DU30, DU35, DU40, and NACA64 from root to tip in the span-wise direction. The turbine is designed to work in an upwind configuration with the nacelle located at 87.5m from the bottom surface and the cylindrical hub diameter of 3m. The CAD description is shown in the Fig. 1.

3.2. Mesh and boundary conditions

The computational mesh is developed with a combination of tetrahedral and hexahedral cells, having a total number of 10×10^6 elements. High-quality prisms cells are generated near the geometrical surfaces to resolve sharp flow gradients. To obtain a thorough estimate of wake deficit in the downstream direction, a block comprising of dense, high-quality hexahedral cells are positioned in the downstream direction as depicted in Fig. 1. A zonal approach is adopted to characterize the rotating (turbine rotor) and stationary (rest of domain) regions (Siddiqui et al., 2014; Tariq Rabbani and Akhtar, 2014; Siddiqui et al., 2013). A *interface* boundary condition is enforced to allow accurate computation of fluxes across two region boundaries. *Inflow* and *outflow* boundary conditions are applied to inlet and outlet boundaries. *No-slip* boundary condition is imposed to turbine geometry and ground surface while a *slip* boundary condition is implemented on lateral/top surfaces of the domain (more information about boundary condition can be found in Jasak (1996)). Fig. 1 outlines the schematic of the CAD model, along with information about the boundary conditions.

3.3. Discretization schemes

The solver is developed in opensource multiphysics toolbox OF® (Jasak, 1996; 5-8 January, 2008). It is based on the FV framework and uses Gauss theorem to discretize spatial derivatives to transform cell center values to face centers. For the discretization of convective terms, a second-order upwind interpolation scheme is employed to calculate the face values. To discretize the diffusive term, a central differencing interpolation scheme with non-orthogonality correction is adopted to attain higher accuracy. The pressure gradient term is handled with the second order least squares interpolation scheme. It is also ensured that the neighboring cell values conform corresponding to the extrapolated face value. To establish continuity of modified pressure, OF® uses an elliptic equation. It involves combining the continuity equation with the divergence of the momentum equation. Both equations (elliptic & momentum equation and turbulence equation), are solved in a segregated manner using the Semi-Implicit Method for Pressure-Linked Equations (SIMPLE) algorithm for steady solutions and a combination of SIMPLE and Pressure Implicit with Splitting of Operator (PISO) for the transient solutions (also known as PIMPLE algorithm). For the discretization of the time derivative, second-order accurate backward Euler scheme is employed.

3.4. Solver settings

The standard operating conditions are chosen for high fidelity simulations with reference fluid density $\rho = 1.225$ kg/m^3, dynamic viscosity $\mu = 1.82 \times 10^{-5}$ kg/m.s incoming wind velocity $U_\infty = 12$ m/s and turbine rotational speed of $\Omega = 0.8$ rad/s. The governing equations are solved using a URANS procedure with k-ω SST turbulence model, while SMI strategy is adopted to handle the rotor modeling. Self adjusting time step procedure is selected to allow time steps to adjust based on Courant number requirements to overcome initial instabilities pertaining to cyclic movement of rotor region. The high fidelity offline simulations are executed on parallel clusters *Vilje* - high performance computing facility at Norwegian University of Science & Technology (NTNU). The mesh is partitioned into eight regions based on SCOTCH (Jasak, 1996) approach, which decomposes mesh block to minimise the number of processor boundaries. Strict emphasis is placed on convergence criterion and residuals of flow quantities are monitored to reach below the levels of 10^{-5} for all flow quantities. The residual are calculated for the matrix system $\mathbf{Ax} = \mathbf{b}$ as outlined by Jasak (1996) in the following way.

$$r = \frac{1}{n}\sum |\mathbf{b} - \mathrm{A}\mathbf{x}| \tag{41}$$

where n is evaluated with residual scaling and using the following normalization

$$n = \sum (|\mathrm{A}\mathbf{x} - \mathrm{A}\overline{\mathbf{x}}| + |\mathbf{b} - \mathrm{A}\overline{\mathbf{x}}|) \tag{42}$$

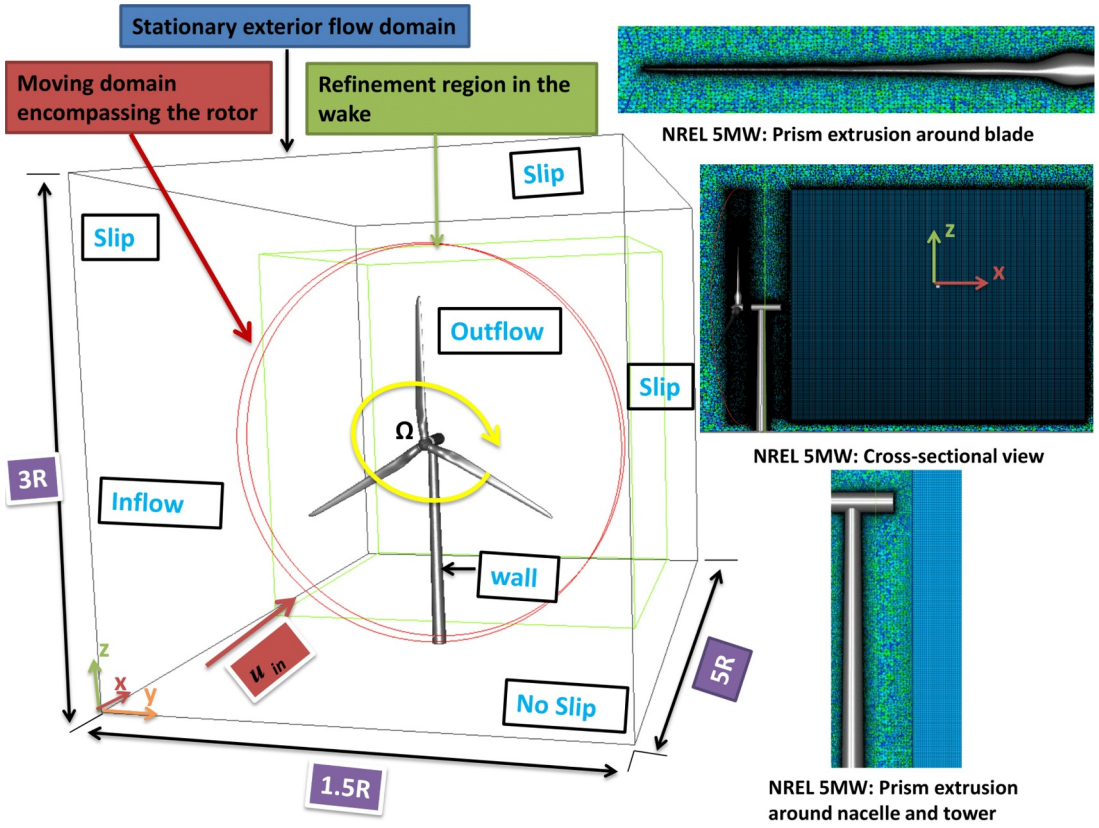

Fig. 1. NREL 5MW: Schematic of computational setup employed with information about boundary conditions. The extent of the domain is 5R × 1.5R × 3R. The computational mesh is composed of tetrahedral and hexahedral elements with high-quality prisms having fifteen successive layers of refinement near the turbine geometry. A zonal approach with an interface boundary is coupling the rotating (rotor) and stationary (rest of the domain) regions. The computational grid consists of 10×10^6 elements.

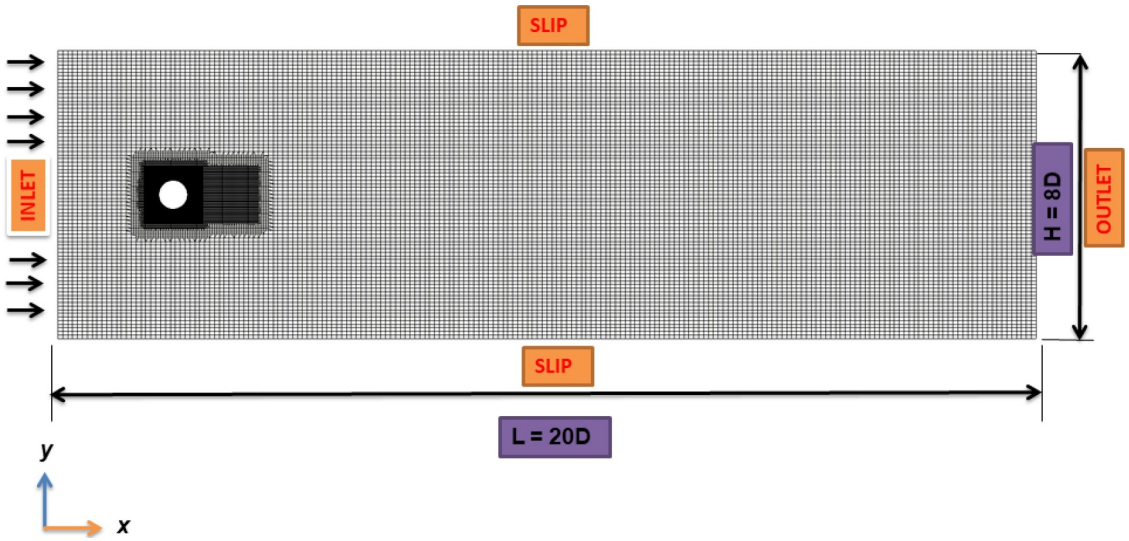

Fig. 2. Cylinder: Schematic of the hexahedral computational mesh used for high-fidelity simulations of the cylinder. The computational domain has a length of 20D and a height of 8D (where D represents the diameter of the cylinder). The mesh has the base refinement of two hundred cells in the x-direction and eighty cells in the y-direction and refined in five successive layers of refinement. The total size of computational grid points elements is 43762.

4. Results and discussions

4.1. Benchmark test case: Flow around a cylinder

The methodology is first tested against a benchmark problem of flow around a cylinder presented in Stabile et al. (2018) with POD-Galerkin approach at a low Re number. Under the present operating condition, both numerical and experimental data are available for the given problem. Validation is conducted under the same computational characteristics of height and width (defined as a function of diameter (D = 0.027 m)) and mesh points (43762 cells). Fig. 2 represents the computaitonal mesh employed along with description of boundary conditions. Viscosity is used as a physical parameter, and high fidelity simulations are performed over five values of the Re = [100, 125, 150,

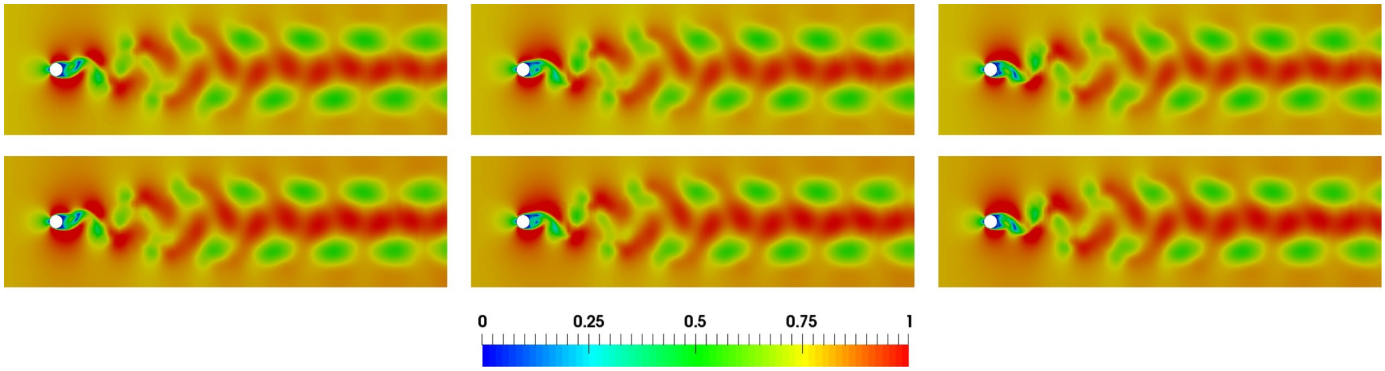

Fig. 3. Cylinder: Comparison of the velocity field (m/s) for high fidelity (HF - top row) and reduced order model (ROM - bottom row) at time instants of t = 190s, 195s, 200s. ROM solution obtained using fifteen modes of velocity. Note: the velocity magnitude is restricted to 0 - 1 m/s to provide better contrast

Table 1
Cylinder: The table outlines the cumulative eigenvalues for flow around cylinder problem against number of modes. Comparison is shown for high fidelity (HF), reduced order model (ROM) and the result of benchmark study (Ref) Stabile et al. (2018) for velocity and pressure flow variables.

N Modes	U - Ref	U - HF	U - ROM	p - Ref	p - HF	p - ROM
1	0.390813	0.391238	0.391576	0.793239	0.797466	0.797466
2	0.598176	0.597255	0.597981	0.85809	0.859376	0.859376
3	0.802176	0.805723	0.80622	0.911636	0.917934	0.917934
4	0.879096	0.87936	0.874914	0.978072	0.975848	0.975848
5	0.949519	0.95003	0.95103	0.98669	0.984727	0.984727
10	0.986025	0.988475	0.989458	0.998307	0.996476	0.996476
15	0.995922	0.997918	0.99884	0.999732	0.999871	0.999871

175, 200] with varying levels of viscosity. Snapshots are collected at each value of Re over 200 s of simulation time. The numerical problem is tested under periodic response conditions between the 190 s and 200 s. Strict emphasis is placed to enable flow to turn into a fully developed state before the ensemble matrix is constructed. The resulting ensemble consists of five hundred snapshots gathered from five different high fidelity simulations captured over an interval of 0.05 s. POD is accomplished over the snapshot ensemble matrix to obtain modes, which are later projected over governing equations to develop ROM for velocity and pressure. The comparison of ROM against high fidelity solution is shown in Fig. 3. The ROM is reconstructed based on the first fifteen modes of velocity and pressure, respectively. Two simulations match well with negligible apparent variations in the underlying flow field. Cumulative eigenvalues depicted in Table 1 represent close agreement and the flow spectrum of velocity and pressure decay close to the rate presented in the benchmark test case. Fig. 4 shows a comparison of lift and drag coefficient for the high fidelity and ROM solutions. The aerodynamic coefficients computed using ROM solutions match within 0.05% of high fidelity simulations and benchmark test case (Stabile et al., 2017a), giving the confidence to scale the procedure to a full-scale turbine.

4.2. NREL 5MW high fidelity simulations validation

The high fidelity numerical simulations of NREL 5MW wind turbine is conducted at full scale at the design operating Tip Speed Ratio (TSR) of 7.5. Validation of high fidelity simulation is performed against benchmarked numerical and analytical solutions available in literature by Jonkman et al. (2005, Tech. Rep. NREL/EL-500-38230); Yu et al. (2011). Independence studies such as grid, time, turbulence model, etc. are conducted to arrive at accurate computational parameters (more details could be retrieved from a previously published article by authors in Siddiqui et al. (2019c)). Total aerodynamic torque transient evolution computed by high fidelity solution using the SMI approach is shown in Fig. 5. In order to validate the torque distribution in the direction of the blade span, the blade is divided into 18 span-wise patches, as presented in Yu et al. (2011). The torque has matched well at most of the patches with minor discrepancies observed at some location (patch 7, 15, 17) along the span. It is believed to happen due to possible differences in the underlying computational mesh resolution or numerical solver settings employed in two studies. The Fig. 5(b) depicts the transient evolution of aerodynamic torque. The plots report initial

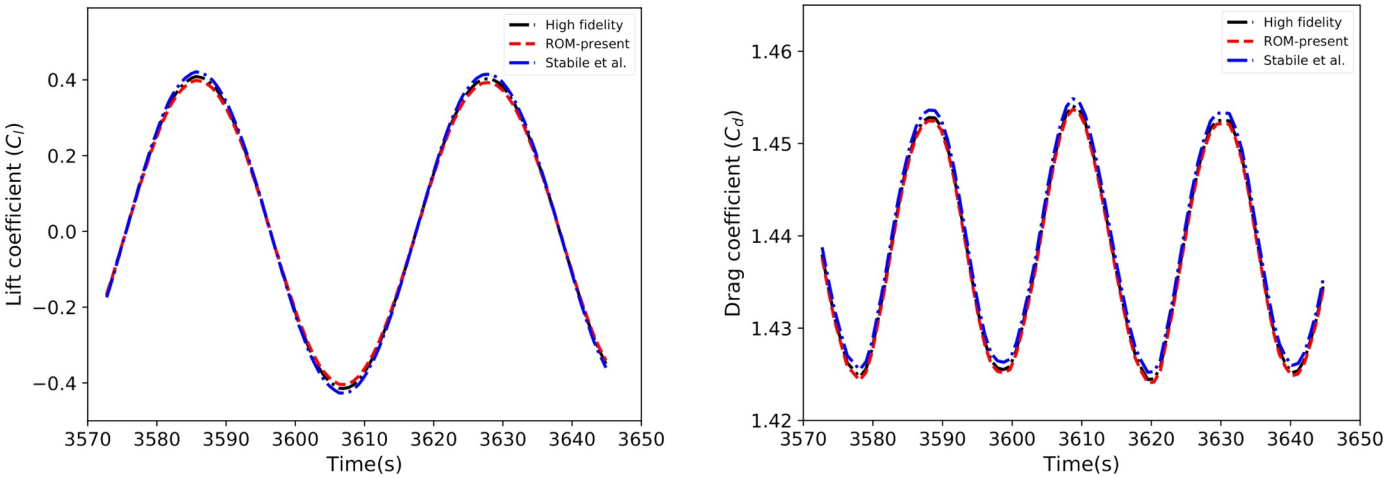

Fig. 4. Cylinder: Comparison of the lift (left) and drag (right) coefficient obtained from high fidelity(HF), reduced order model (ROM) against the benchmark results (Stabile et al., 2018). The solution from ROM is computed using fifteen modes.

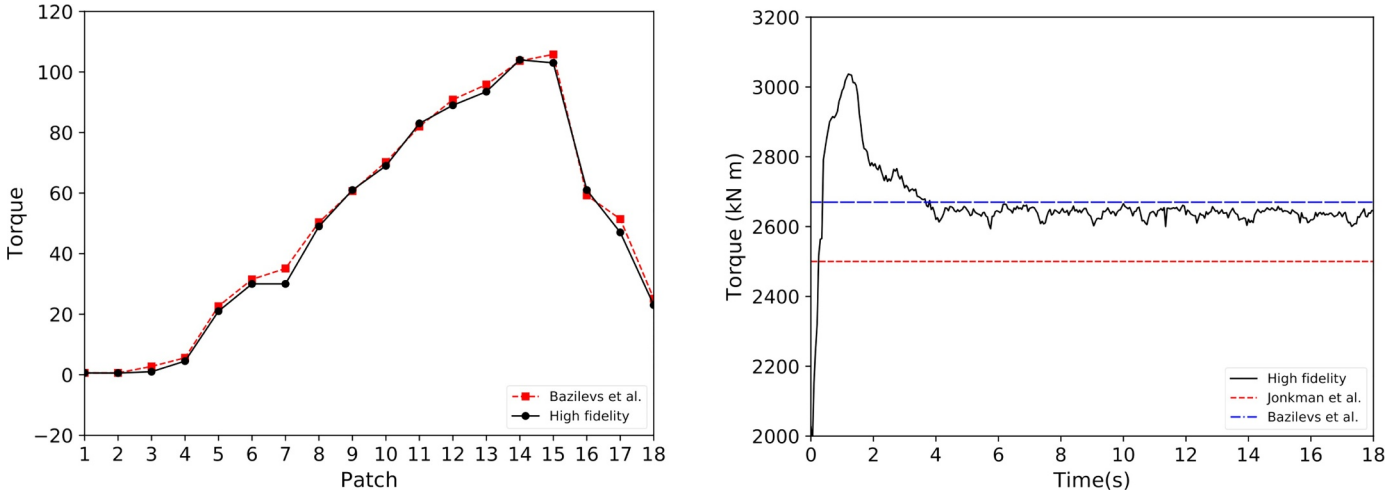

Fig. 5. NREL 5MW: Transient evolution of aerodynamic torque of wind turbine compared against reference solutions of (Bazilevs et al., 2011; Jonkman et al., 2009, Tech. Rep. NREL/TP-500e38060). (left) the blade has been divided into 18 patches, and the torque contribution is accounted for each at t = 0.8 s. (right) Initial instabilities are observed in torque evolution which smothered out with more turbine rotations.

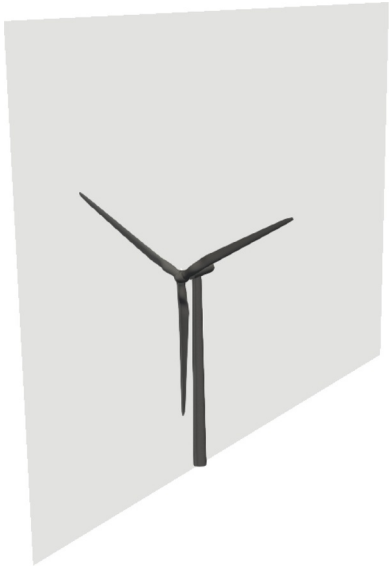

Fig. 6. NREL 5MW: Schematic of computational planes passing through the turbine. This is used to store high fidelity solutions to develop the ensemble matrix over which POD procedure is applied to obtain energy-rich significant modes.

Table 2
NREL 5MW: The table outlines the first seventy cumulative eigenvalues for the velocity and pressure against number of modes.

N Modes	Velocity $\sum_{i=1}^{70}\lambda_i$	Pressure $\sum_{i=1}^{70}\lambda_i$
1	0.215145	0.656455
15	0.720673	0.817616
30	0.819303	0.860142
45	0.930040	0.959034
60	0.985422	0.989752
70	0.997549	0.999151

fluctuations in torque value for high fidelity simulations, which happen because of initial instabilities in the numerical solutions subjected to the turbine rotation. The torque eventually settles at a stationary value of approximately 2,570 kN m, which is within 3% of the reference (Jonkman et al., 2005, Tech. Rep. NREL/EL-500-38230). This

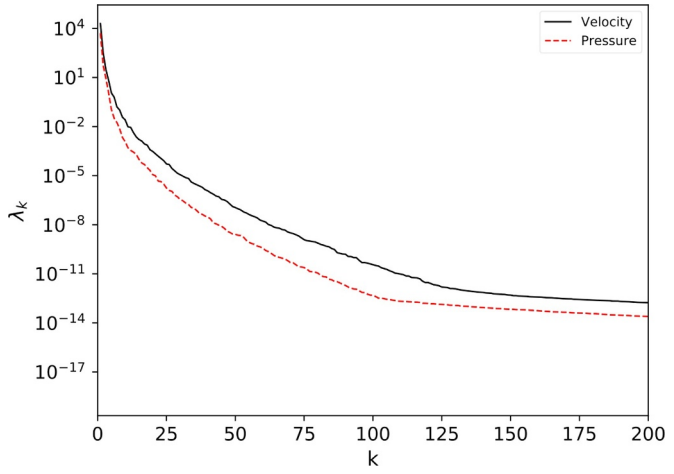

Fig. 7. NREL 5MW: Spectrum of velocity and scalar pressure for first two hundred modes. The decay in values is observed to be rapid for the first seventy modes, after which the behaviour seems to flattens out.

value is also close to the results of (Yu et al., 2011), which reports an average torque value of 2, 670 kN m using numerical simulations. The validation problem has given solid grounds for high fidelity numerical procedure, thereby providing confidence to ensemble accurate flow snapshot matrices for ROMs in the upcoming section.

4.3. ROM implementation

Once the high fidelity simulations are tested against benchmarked solutions, the offline phase of ROM simulations is conducted in OF®. The velocity, scalar pressure and face flux fields are extracted from the high fidelity simulations at various time instants. The choice of velocity is crucial at this point as it represents a direct measure of the total kinetic energy present in the flow field. This is also justified by the fact that one of the motivations of the present study, as mentioned earlier in the introduction, is to analyze the wake evolution downstream from both high fidelity and ROM solutions. Fig. 6 represents the plane used to construct an ensemble of high fidelity snapshots that are collected after initial numerical fluctuations arising from turbine rotation have been suppressed. The snapshots are acquired at a rate of 0.05 s, and a total of 1000 snapshots are accumulated over three turbine cycles.

For the generation of POD basis and construction of ROM matrices,

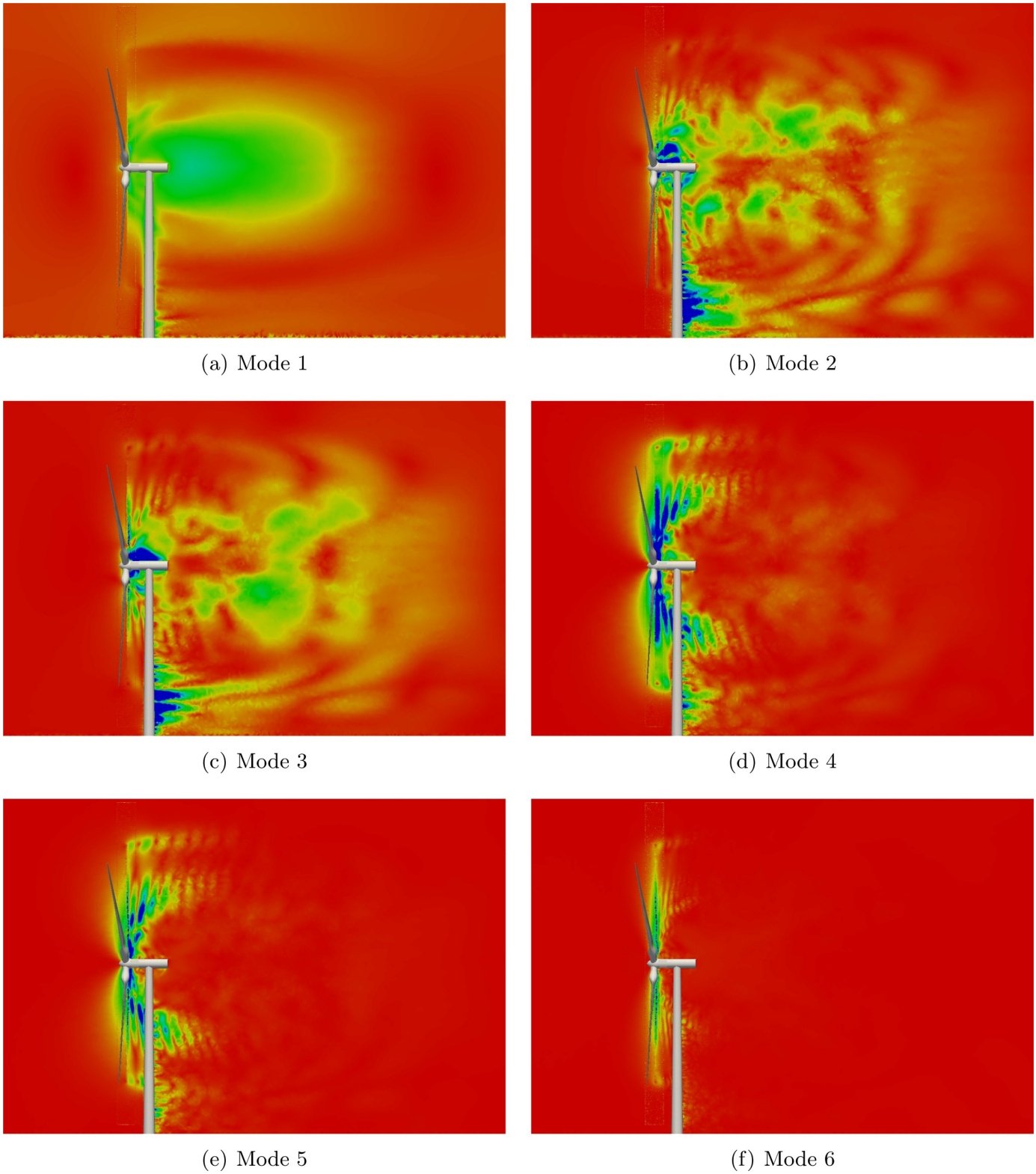

Fig. 8. NREL 5MW: The first six POD modes for the wind turbine. Modes are sorted in a hierarchical manner of high to low energetic states. Along with representing the distribution of energy in the flow field the modes also highlight the spatial coherence of large and small scale eddies.

python is employed. Given the two platforms, python and OF® (C++ library), share common similarities of object-oriented programming framework which enable to compute direct solutions of ROM matrices in the online stage. Moreover, python's powerful and efficient capabilities allowed handling large sets of data matrices. A standard solver for Ordinary Differential Equation (ODE) using the Runge-Kutta method is implemented in python to solve the ROM system in the online phase. The solution is computed to relative tolerance levels of 1×10^{-5} for quantities of interests.

Table 3
NREL 5MW: Illustration of speedups achieved from ROM using different number of modes compared to high fidelity simulations. It shows that by employing fewer degrees of freedom massive speedup are achieved with significant reduction in accuracy. *Speedup* is defined as time taken for high-fidelity divided by the time taken for the reduced solution on average. *Relative error* is absolute L^2 norm error divided by L^2 norm of the velocity of the reference/high-fidelity solution.

	Modes	Speedup	Relative error (Velocity)
High-fidelity	200	1	0
Reduced Order Model	15	18,842	1.3×10^{-1}
	30	7,899	9.1×10^{-2}
	45	5,433	7.5×10^{-2}
	60	4,332	6.1×10^{-3}
	70	3,285	4.7×10^{-3}

4.4. POD modes

The high fidelity snapshots ensemble collected at various time instances for velocity over multiple turbine cycles are applied with the POD in the offline stage to generate an optimal basis according to the procedure described in Section 4.4. Fig. 8 represent the qualitative description of modes that results after POD procedure. The modes are sorted in a hierarchical manner of high to low energetic states of the system. In addition to representing the distribution of energy, the acquired modes also provide a brief description of the spatial evolution of underlying dominant scales of motion. It can be seen that the first mode illustrates the mean flow behavior of the flow field around the turbine and comprises almost 21% of the system's energy. A significant portion of this energy is seen to be concentrated in the downstream wake adjacent to the turbine structure. In the following modes, the large scale structures are observed to become less pronounced and distinct smaller structures start to appear. Thus the procedure has segregated wakes energy into individual contributions from underlying scales of large and small coherent structures. It is evident that initial modes fully capture the mean flow field structure, while higher modes contain energy corresponding to coherent scales that emanate primarily from the turbine blades. According to the Fig. 8, flow coherence close to the turbine blade starts to become more pronounced from mode number of four and above. The subsequent modes continue to represent small scales structures present in the flow field. In general, the POD procedure has provided an optimal linear subspace for the present wind turbine flow problem by working as an energy filter and identifying large coherent structures, while bypassing less coherent structures to the lower modes (H., 2000; Gamard and George, 2002).

In the context of the aforementioned discussion, once notice that POD procedure has successfully generated reduced basis while limiting the degrees of freedom of high fidelity problem to fewer modes that constitute of a significant portion of energy governed by corresponding eigenvalues (first seventy cumulative eigenvalues with an increment of fifteen shown in Table 2). This reflects that almost seventy modes capture almost 99% of systems energy. In addition to providing the basis for the successful construction of ROM matrices, modes obtained through POD has also provided a rather intricate assessment of the composition of the flow and the underlying scales of motion.

4.5. Spectrum

Fig. 7 depicts the spectrum of the velocity and pressure field plotted over the first two hundred modes (quantitative data tabulated in Table 2). The spectrum outlines the number of modes required for suitable construction of ROM with corresponding energy content for velocity and pressure. According to the plot, scalar pressure is observed to decay faster than the velocity. It is apparent that the first seventy modes account for a significant portion of energy. Additional modes can be selected to improve the overall accuracy of ROM for the given wind turbine related problem. However, it may rather come at the expense of increasing the computational effort, which is not of interest at this point.

4.6. ROM reconstruction - wake deficit

After the completion of the offline phase, ROM matrices are formulated according to the procedure described in Section 4.4. The ROM simulations are executed for time instants $t = 0.8$ s that are considered in the high fidelity solution benchmarked studies. Here the ROM capability is tested for reproducing the outputs against full order simulations. Both the ROM simulation and the high fidelity simulation are formulated under similar conditions to avoid inconsistencies that arise due to the change in operating procedures. ROM simulation is performed with an increasing number of modes starting from one until seventy modes. Table 3 reports modes against *speedups* and *relative error* of ROM and high fidelity simulations. It depicts that by employing

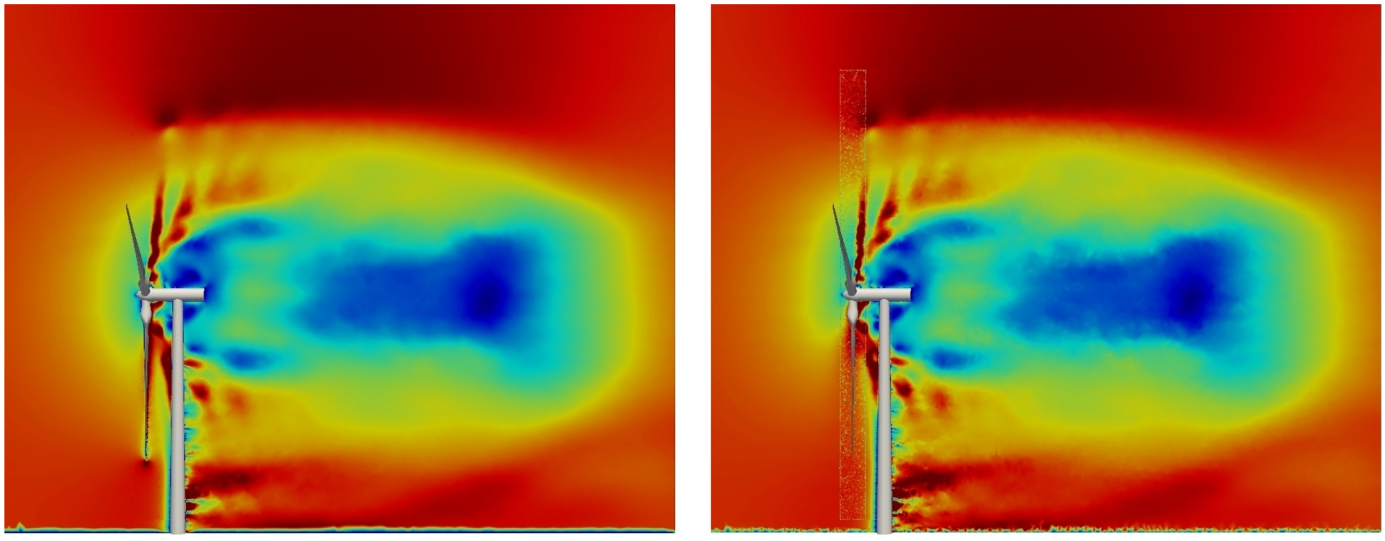

Fig. 9. NREL 5MW: Contours of the velocity field on a plane passing through the center of the turbine rotor (inertial reference frame) (left) high fidelity simulation (right) reconstruction of velocity field by reduced order model (ROM) using 25 POD modes. It is interesting to observe that ROM has captured adequately small scales present in flow field (tip and hub vortices). Note: the velocity magnitude is restricted to 0–20 m/s to provide better contrast.

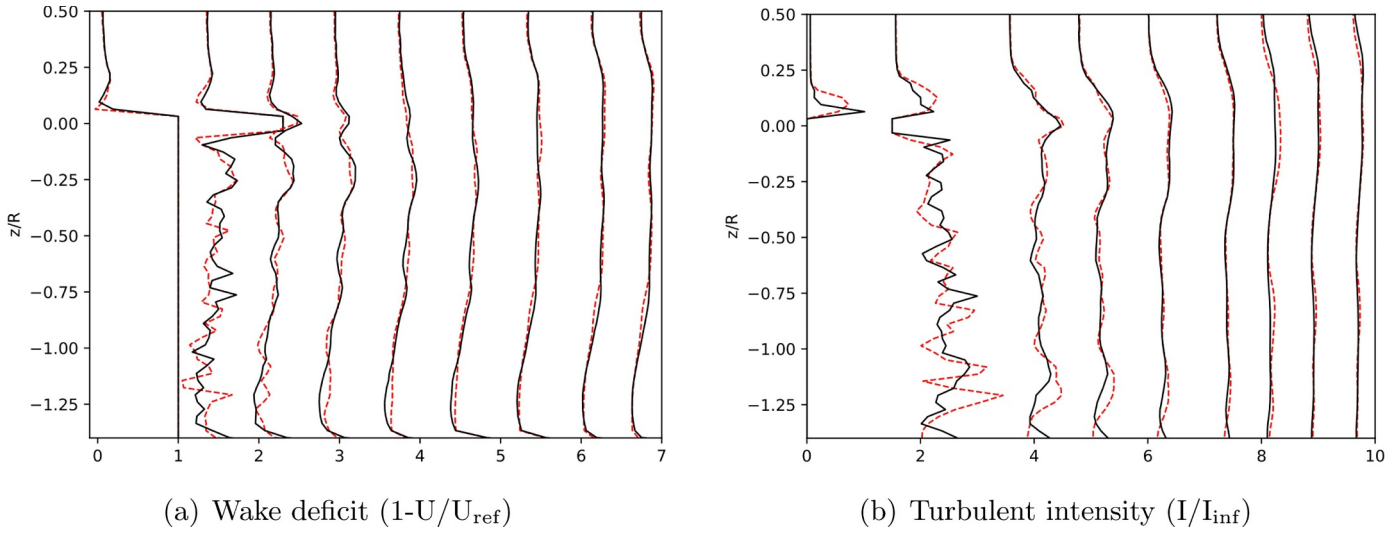

Fig. 10. NREL 5MW: Wake deficit and turbulent intensity in vertical direction for high fidelity (solid line) and reduced order model (dotted line) at successive locations in downstream direction (0.15R, 0.30R, 0.45R, 0.60R, 0.90R, 1.30R, 2.00R, 2.50R, 3.00R from hub). Note*: Successive profiles have been offset for better clarity.

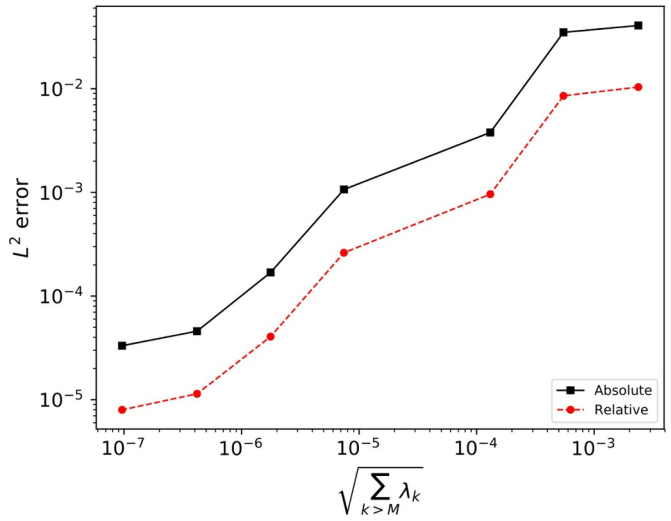

Fig. 11. NREL 5MW: Absolute and relative error analysis for the velocity field. The L^2 norm of the error is plotted against cumulative eigenvalues. The marks are given for the first mode and then in intervals of fifteen modes.

fifteen modes, massive speedup of 18,842 is observed from the present ROM methods, with an accuracy of approximately 13% measured in L^2 norm. Given the lower accuracy levels in comparison to the ones that were aimed, thirty and forty-five modes are tested, which provides a speedup of approximately 7,899 and 5,433 along with corresponding relative errors of 9.1% and 7.5% for velocity respectively. Further, employing seventy modes results in speeds of 3,285 with an efficiency of 4.7%, which is believed to be accurate enough (since less than 5% accuracy is targeted) for the present investigation.

The qualitative comparison between the high fidelity and ROM simulations is depicted in Fig. 9. It shows that the overall dynamics in flow field has been captured with reasonable accuracy employing seventy POD modes in ROM. The central wake (region shown in blue color adjacent to the turbine) along with small scale eddies (tip/hub vortices), which are often quantities of interests in studies related to wake dynamics, are reconstructed successfully. Given the lower dimension of the basis used in the ROM, few minor differences are anticipated. However, considering the acquired accuracy and minimal computational times, such differences seem negligible from an engineering standpoint.

The quantitative comparison between the ROM against the high fidelity solutions is conducted realizing that the real purpose of ROM is not to approximate a physical system better than its high fidelity counterpart, that is

$$\|\text{Physical}(\boldsymbol{\mu}) - \text{ROM}(\boldsymbol{\mu})\| = \|\text{Physical}(\boldsymbol{\mu}) - \text{HF}(\boldsymbol{\mu})\| + \|\text{HF}(\boldsymbol{\mu}) - \text{ROM}(\boldsymbol{\mu})\|$$

for what concerns the present investigation, the focus primarily is to evaluate $\|\text{HF}(\boldsymbol{\mu}) - \text{ROM}(\boldsymbol{\mu})\|$ rather than $\|\text{Physical}(\boldsymbol{\mu}) - \text{HF}(\boldsymbol{\mu})\|$, which has been the main focus of many previous studies conducted in the literature. For quantitative comparison of the wake, ROM solutions are compared in Fig. 10 against high fidelity solutions as published in study (Siddiqui et al., 2019c), previously performed under similar operating conditions. Wake deficit and turbulent intensity levels are compared at nine locations (0.15R, 0.30R, 0.45R, 0.60R, 0.90R, 1.30R, 2.00R, 2.50R, 3.00R) starting from central hub in the streamwise direction at t = 0.8 s. It is observed that the ROM solution manage to capture the wake deficit and turbulent intensity (Siddiqui et al., 2015b) pattern behind the wind turbine in a realistic manner. Full-scale modeling of turbine geometry (nacelle and monopole) has given rise to complex flow configuration, causing oscillations in the profiles adjacent to the structure. ROM manages to capture these profiles adequately adjacent to the turbine; however, a rather good match is observed away from the turbine where sharp variation in the flow field seems to settle down due to recovery of wake strength owing to molecular diffusion. From the standpoint of accuracy, the ROM has captured reasonably the wake deficit and turbulent intensity profiles corresponding to its high fidelity counterparts.

4.7. L^2 error

L^2 error of absolute and relative velocity between high fidelity and ROM versus the decay of eigenvalue distribution is displayed in Fig. 11. To study error accumulation in higher modes, the plot show modes starting from a single-mode with an increment of fifteen modes. The L^2 error convergence follows a similar curve for absolute and relative error and a monotonic overall drop is observed against the cumulative eigenvalues data. No significant decrease in error value is reported after seventy modes, which represent that ROM solution will not benefit from the use of higher modes to approximate its high-fidelity counterpart with greater accuracy; rather, it will contribute directly to

increasing computational effort.

In this work, a proper orthogonal decomposition - Galerkin framework was tested in a finite volume setting to evaluate the prediction capabilities of a reduced order model by determining wake characteristics for flow around an NREL 5MW wind turbine. High fidelity simulations were conducted by Unsteady Reynolds Average Navier Stokes procedure using opensource code OpenFOAM® and the solutions were benchmarked against the available results presented in the literature. A proper orthogonal decomposition technique was applied to obtain significant modes, which were projected onto the governing system to obtain the reduced-order model. A detailed quantitative and qualitative comparison of modes and reconstructed velocity field was conducted. The reduced order model has successfully captured the coherent structures of turbulence along with accurate estimates of wake deficit and turbulent intensity on a plane passing through the turbine center. The results showed that approximately seventy modes comprise of 99% of systems energy with corresponding speeds of 3,285 and a relative velocity error of 4.7% in L^2 norm.

In the future, the work will be explored further to account for the three-dimensional effects of flow in the construction of the reduced order model, which certainly poses a challenge at present from the standpoint of computational requirements. Other interesting aspects could be to study the entire wind park in a high fidelity context to enable accurate and realistic estimates of offshore wind farms in a relatively short time.

CRediT authorship contribution statement

M. Salman Siddiqui: Conceptualization, Methodology, Writing - original draft. **Sidra Tul Muntaha Latif:** Software, Methodology, Data curation, Writing - original draft. **Muhammad Saeed:** Software, Writing - review & editing. **Muhammad Rahman:** Investigation, Writing - review & editing. **Abdul Waheed Badar:** Investigation, Writing - review & editing. **Syed Maaz Hasan:** Validation, Writing - review & editing.

Declaration of Competing Interest

The authors declare that they have no known competing financial interests or personal relationships that could have appeared to influence the work reported in this paper.

References

Akhtar, I., Marzouk, O.A., Nayfeh, A.H., 2009. A van der Pol-Duffing oscillator model of hydrodynamic forces on canonical structures. J. Comput. Nonlinear Dyn. 4 (4).

Akhtar, I., Mittal, R., Lauder, G.V., Drucker, E., 2007. Hydrodynamics of a biologically inspired tandem flapping foil configuration. Theoret. Comput. Fluid Dyn. 21 (3), 155–170.

Aubry, N., 1991. On the hidden beauty of the proper orthogonal decomposition. Theoret. Comput. Fluid Dyn. 2 (5), 339–352.

Bakewell, H.P., Lumley, J.L., 1967. Viscous Sublayer and Adjacent Wall Region in Turbulent Pipe Flow. Phys. Fluids 10, 1880–1889.

Ballarin, F., Manzoni, A., Quarteroni, A., Rozza, G., 2015. Supremizer stabilization of POD-Galerkin approximation of parametrized steady incompressible Navier-Stokes equations. Int. J. Numer. MethodsEng. 102 (5), 1136–1161.

Ballarin, F., Manzoni, A., Quarteroni, A., Rozza, G., 2015. Supremizer stabilization of POD galerkin approximation of parametrized steady incompressible Navier-Stokes equations. Int. J. Numer. MethodsEng. 102 (5), 1136–1161.

Bastine, D., Witha, B., Wchter, M., Peinke, J., 2014. POD analysis of a wind turbine wake in a turbulent atmospheric boundary layer. J. Phys.: Conf. Ser. 524, 12153.

Bazilevs, Y., Hsu, M.C., Akkerman, I., Wright, S., Takizawa, K., Henicke, B., Spielman, T., Tezduyar, T.E., 2011. 3D simulation of wind turbine rotors at full scale. part I: Geometry modeling and aerodynamics. Int. J. Numer. MethodsFluids 65 (1–3), 207–235.

Bergmann, M., Bruneau, C., Iollo, A., 2009. Enablers for robust POD models. J. Comput. Phys. 228 (2), 516–538.

Berkooz, G., Holmes, P., Lumley, J.L., 1993. The proper orthogonal decomposition in the analysis of turbulent flows. Annu. Rev. Fluid Mech. 25 (1), 539–575.

Bizon, K., Continillo, G., 2012. Reduced order modelling of chemical reactors with recycle by means of POD-penalty method. Comput. Chem. Eng. 39, 22–32.

Fonn, E., Tabib, M., Siddiqui, M.S., Rasheed, A., Kvamsdal, T., 2017. A step towards reduced order modelling of flow characterized by wakes using proper orthogonal decomposition. Elsevier Energy Procedia 137, 452–459.

Gamard, S., George, W.K., 2002. Application of a slice proper orthogonal decomposition to the far field of an axisymmetric turbulent jet. Phys. Fluids 14, 2515.

H., C.J., 2000. Reconstruction of the global velocity field in the axisymmetric mixing layer utilizing the proper orthogonal decomposition. J. Fluid Mech. 418, 137.

H.Kazimierczuk, A., 2019. Wind energy in Kenya: a status and policy framework review. Renew. Sustain. Energy Rev. 107, 434–445.

Hsu, M.C., Akkerman, I., Bazilevs, Y., 2014. Finite element simulation of wind turbine aerodynamics: validation study using NREL phase VI experiment. Wind Energy 17 (3), 461–481.

Jasak, H., 1996. Error analysis and estimation in the finite volume method with applications to fluid flows. Imperial College, University of London.

Jasak, H., 5-8 January, 2008. Dynamic mesh handling in openfoam. 47th AIAA Aerospace Sciences Meeting Including the New Horizons Forum and Aerospace Exposition. 52. pp. (AIAA2009–341).

Jonkman, J., Marshal, L., Buhl, J., 2005. Fast users guide.Fast users guide. Tech. Rep. NREL/EL-500-38230

Jonkman, J.M., Butterfield, S., Musial, W., Scott, G., 2009. Definition of a 5MW reference wind tturbine for offshore system development.Definition of a 5MW reference wind tturbine for offshore system development. Tech. Rep. NREL/TP-500e38060

Khalid, M.S.U., Rabbani, T., Akhtar, I., Durrani, N., Siddiqui, M.S., 2014. Reduced-order modeling of torque on a vertical-axis wind turbine at varying tip-speed ratios. https://doi.org/10.1115/1.4028064.

Khalid, S., Rabbani, T., Akhtar, I., Durrani, N., Siddiqui, M.S., 2015. Reduced-order modeling of torque on a vertical-axis wind turbine at varying tip-speed ratios. ASME J. Comput. Nonlinear Dyn. 10 (CND-14-1055), 41012.

Krogstad, P.A., Saetran, L., 2012. An experimental and numerical study of the performance of a model turbine. Wind Energy 15 (3), 443–457.

Kumar, M., Singh, A.K., Srivastava, A., 2013. Various newton-type iterative methods for solving nonlinear equations. J. Egyptian Math. Soc. 21 (3), 334–339.

Lorenzi, S., Cammi, A., Luzzi, L., Rozza, G., 2016. Balanced Model Reduction via the Proper Orthogonal Decomposition. Comput. Methods Appl. Mech.Eng. 311, 151–179.

Lorenzi, S., Cammi, A., Luzzi, L., Rozza, G., 2016. POD-galerkin method for finite volume approximation of Navier-Stokes and RANS equations. Comput. Methods Appl. Mech.Eng. 311, 151–179.

Tabib, M.,, K., E.F.A.R.T.,, Siddiqui, M.S.,, 2017. Near wake region of an industrial scale wind turbine: comparing LES-ALM with LES-SMI simulations using data mining (POD). Journal of Physics: Conference Series. 854. IOP Publishing, pp. 012044.

Menter, F., 1994. Two-equation eddy-viscosity turbulence models for engineering applications. AIAA J. 32, 1598–1605.

Menter, F., 2009. Review of the shear-stress transport turbulence model experience from an industrial perspective. Int. J. Comput. Fluid Dyn. 23, 305–316.

Milosevic, M., 2018. Convergence and almost sure polynomial stability of the backward and forward backward euler methods for highly nonlinear pantograph stochastic differential equations. Math. Comput. Simul. 150, 25–48.

Mo, J.O., Choudhry, A., Arjomandi, M., Lee, Y.H., 2013. Large eddy simulation of the wind turbine wake characteristics in the numerical wind tunnel model. J. Wind Eng. Ind.Aerodyn. 112, 11–24.

Patera, A.T., Rønquist, E.M., 2007. Reduced basis approximation and a posteriori error estimation for a boltzmann model. Comput. Methods Appl. Mech.Eng. 196 (29), 2925–2942.

Rozza, F.B.A.M.A.Q.G., 2015. Supremizer stabilization of POD-Galerkin approximation of parametrized Navier-Stokes equations. . J. Numer. MethodsEng. 102 (5).

Siddiqui, M.S., Durrani, N., Akhtar, I., 2013. Numerical study to quantify the effects of struts and central hub on the performance of a three dimensional vertical axis wind turbine using sliding mesh. ASME 2013 Power Conference. American Society of Mechanical Engineers Digital Collection.

Siddiqui, M.S., Durrani, N., Akhtar, I., 2015. Quantification of the effects of geometric approximations on the performance of a vertical axis wind turbine. Renew. Energy 74 (0), 661–670.

Siddiqui, M.S., Fonn, E., Kvamsdal, T., Rasheed, A., 2019. Finite-volume high-fidelity simulation combined with finite-element-based reduced-order modeling of incompressible flow problems. Energies 12 (7), 1271.

Siddiqui, M.S., Hasan, S.M., Hasan, S.M., 2014. Optimized design of a straight blade urban roof top vertical axis wind turbine. 2014 International Conference on Energy Systems and Policies (ICESP). IEEE, pp. 1–10.

Siddiqui, M.S., Rasheed, A., Kvamsdal, T., 2019. Validation of the numerical simulations of flow around a scaled-down turbine using experimental data from wind tunnel. Wind Struct.Int. J. 29 (4), 405–416.

Siddiqui, M.S., Rasheed, A., Kvamsdal, T., 2020. Numerical assessment of rans turbulence models for the development of data driven reduced order models. Ocean . 196, 106799.

Siddiqui, M.S., Rasheed, A., Kvamsdal, T., Tabib, M., 2015. Effect of turbulence intensity on the performance of an offshore vertical axis wind turbine. Energy Procedia 80, 312–320.

Siddiqui, M.S., Rasheed, A., Kvamsdal, T., Tabib, M., 2017. Influence of tip speed ratio on wake flow characteristics utilizing fully resolved CFD methodology. J. Phys.: Conf. Ser. 854 (1), 12043.

Siddiqui, M.S., Rasheed, A., Kvamsdal, T., Tabib, M., 2017. Quasi-static and dynamic numerical modeling of full scale NREL 5MW wind turbine. Energy Procedia 137, 460–467.

Siddiqui, M.S., Rasheed, A., Tabib, M., Fonn, E., Kvamsdal, T., 2017. On interactions between wind turbines and the marine boundary layer. ASME 2017 36th International Conference on Ocean, Offshore and Arctic Engineering. American Society of Mechanical Engineers Digital Collection.

Siddiqui, M.S., Rasheed, A., Tabib, M., Kvamsdal, T., 2016. Numerical analysis of NREL 5MW wind turbine: astudy towards a better understanding of wake characteristic and torque generation mechanism. J. Phys.: Conf. Ser. 753 (3), 32059.
Siddiqui, M.S., Rasheed, A., Tabib, M., Kvamsdal, T., 2019. Numerical investigation of modeling frameworks and geometric approximations on nrel 5mw wind turbine. Renew. Energy 132, 1058–1075.
Siddiqui, M.S., Rasheed, A., Tabib, M., Kvamsdal, T., January 5-11, 2017. Numerical modeling framework for wind turbine analysis & atmospheric boundary layer interaction. 35th Wind Energy Symposium AIAA SciTech Forum.
Sirovich, L., 1987. Turbulence and the dyanmics of coherent structures. Q. Appl. Math. 45, 561–590.
Sørensen, N.N., Zahle, F., 2016. Simulations of wind turbine rotor with vortex generators. J. Phys.: Conf. Ser. (Online) 753.
Stabile, G., G.Matthies, H., Borri, C., 2018. A novel reduced order model for vortex induced vibrations of long flexible cylinders. Ocean Eng. 156, 191–207.
Stabile, G., Hijazi, S., Lorenzi, S., Mola, A., Rozza, G., 2017. Advances in reduced order modelling for CFD: vortex shedding around a circular cylinder using a POD-galerkin method. Commun. Appl. Ind. Math.
Stabile, G., Hijazi, S., Mola, A., Lorenzi, S., 2017. POD-Galerkin reduced order methods for CFD using finite volume discretisation: vortex shedding around a circular cylinder. Commun. Appl. Ind. Math. 8 (1), 210–236.
Tabib, M., Rasheed, A., Siddiqui, M.S., Kvamsdal, T., 2017. A full-scale 3D vs 2.5D vs 2D analysis of flow pattern and forces for an industrial-scale 5MW NREL reference windturbine. Energy Procedia 137, 477–486.
Tabib, M., Siddiqui, M.S., Rasheed, A., Kvamsdal, T., 2017. Industrial scale turbine and associated wake development-comparison of RANS based actuator line vs sliding mesh interface vs multiple reference frame method. Energy Procedia 137, 487–496.
Tallet, A., Allery, C., Leblond, C., Liberge, E., 2015. A minimum residual projection to build coupled velocity-pressure POD-ROM for incompressible Navier-Stokes equations. Commun. Nonlinear Sci. Numer.Simul. 22, 909–932.
Tariq Rabbani, M.S.S., Akhtar, I., 2014. Reduced order modeling of loads on a vertical-axis wind turbine. Applied Sciences and Technology (IBCAST), 2014 11th International Bhurban Conference. IEEE, pp. 298–303.
Troldborg, N., Zahle, F., Sørensen, N.N., 2015. Simulation of a MW rotor equipped with vortex generators using CFD and an actuator shape model. Proceedings of 53rd AIAA Aerospace Sciences Meeting, American Institute of Aeronautics & Astronautics.
Yu, G., Shen, X., Zhu, X., Du, Z., 2011. An insight into the separate flow and stall delay for HAWT. Renew. Energy 36 (1), 69–76.
Zahoor, R., Bajt, S., Ŝarler, B., 2018. Influence of gas dynamic virtual nozzle geometry on micro-jet characteristics. Int. J. Multiph. Flow 104, 152–165.
Zahoor, R., Belšak, G., Bajt, S., Ŝarler, B., 2028. Simulation of liquid micro-jet in free expanding high-speed co-flowing gas streams. Microfluid Nanofluid 22(7).